Journal of Magnetism and Magnetic Materials 323 (2011) 290–296

Contents lists available at ScienceDirect

Journal of Magnetism and Magnetic Materials

journal homepage: www.elsevier.com/locate/jmmm

Structural and magnetic study of Mo-doped FINEMET

J.M. Silveyra [a,*], V.J. Cremaschi [a,b], D. Janičkovič [c], P. Švec [c], B. Arcondo [a]

[a] Laboratorio de Sólidos Amorfos, INTECIN, Facultad de Ingeniería, Universidad de Buenos Aires-CONICET, Paseo Colón 850, (C1063ACV) Buenos Aires, Argentina
[b] Miembro de la Carrera del Investigador del CONICET, Argentina
[c] Institute of Physics, Slovak Academy of Sciences, Dúbravská cesta 9, 845 11 Bratislava, Slovakia

ARTICLE INFO

Article history:
Received 27 July 2010
Received in revised form
8 September 2010
Available online 22 September 2010

Keywords:
Nanocrystalline alloy
FINEMET
Mössbauer spectroscopy
Magnetic moment

ABSTRACT

In this paper, a study of the structural and the magnetic correlation of the crystalline and amorphous phases in the nanocrystalline system $Fe_{73.5}Si_{13.5}B_9Nb_{3-x}Mo_xCu_1$ ($x=0$, 1.5, 2, 3) was made. By means of Mössbauer spectroscopy, simple mass balance considerations and density measurements, both phases fractions and chemical compositions were calculated (in at%, wt% and vol%). Then, quasistatic magnetic measurements and *ab initio* calculations were used in a magnetic balance model in order to estimate the magnetic contribution of the remaining amorphous phase, which was compared to that of as-quenched amorphous samples of the same composition. The difference in both magnitudes showed the influence of penetrating fields and that these became more important for higher crystalline fractions.

1. Introduction

Over the last two decades, soft magnetic nanocrystalline alloys have led to an increasing interest for both scientific and technological purposes due to their two-phase structure and excellent magnetic properties. The first system was developed by Yoshizawa et al. [1] and was called FINEMET ($Fe_{73.5}Si_{13.5}B_9Nb_3Cu_1$). The nanocrystallization of Fe–Si phase is obtained after a controlled annealing of amorphous samples: Cu increases the nucleation rate of Fe–Si nanocrystals, whereas Nb prevents the grain's growth [2].

A key issue in the understanding of the magnetic behaviour of nanocrystalline systems is the correlation between the magnetization and the structure of the crystalline grains and the remaining amorphous matrix. Among the relevant parameters, which govern the magnetic behaviour of nanocrystalline alloys, are the amorphous and crystalline fractions and the composition of both phases.

With the aim of further improving the soft magnetic properties and reducing costs, a FINEMET series in which Nb was replaced by Mo was prepared. The consequences in the phase transformations caused by the substitution were studied in Ref. [3] and the magnetostrictive properties were reported in Ref. [4].

In this paper, from ^{57}Fe Mössbauer spectra fittings, simple mass balance considerations and density measurements, the proportions of the two phases in the nanocrystalline alloys $Fe_{73.5}Si_{13.5}B_9Nb_{3-x}Mo_xCu_1$ were calculated (in at%, wt% and vol%) as well as their chemical compositions. Then, from *ab initio* calculations for the $Fe_{1-x}Si_x$ system, the magnetic moment of the grains was estimated. The magnetic flux density of the nanocrystalline alloys was measured with a quasistatic method. Finally, from a simple magnetization balance model, the magnetic contribution of the remaining amorphous matrices was estimated and compared with the saturation flux density measurements of as-quenched samples of the same chemical compositions.

2. Mössbauer spectrometry applied to FINEMET alloys

Mössbauer studies have been widely performed to characterize the amorphous and Fe–Si crystalline FINEMET phases. In solid state, the solubility of silicon in the BCC iron structure is very high. In the iron-rich region of the Fe–Si phase diagram (Fig. 1) three different phases are formed depending on the silicon content: $\alpha \rightarrow \alpha' \rightarrow \alpha''$ [5,6]. The α''-phase has a DO3 structure (Fm3m space group), whose lattice parameter is roughly twice as large as that of α-Fe. The unit cell consists of 16 atoms occupying 4 sites arranged regularly along the body diagonal: A, B, C and D (Fig. 2). In stoichiometric Fe_3Si, Fe atoms occupy A, B and C sites, whereas Si atoms occupy only D sites (preventing from a metalloid pair formation at a nearest-neighbour distance). A and C are sites structurally and magnetically equivalent and have 4 Fe [B] and 4 Si [D] atoms as nearest-neighbours (NN). B sites have 8 Fe [A,C] atoms as NN, just like in elemental BCC α-Fe. The α′-phase has a B2 structure (Pm3m space group) and Si atoms can occupy B and D sites, or, if seen as a BCC structure, the centred atom of the cell. The α-phase has an A2 structure (Im3m space group), in which Si atoms occupy all sites with the same probability.

* Corresponding author.
E-mail address: jsilveyra@fi.uba.ar (J.M. Silveyra).

0304-8853/$ - see front matter © 2010 Elsevier B.V. All rights reserved.
doi:10.1016/j.jmmm.2010.09.019

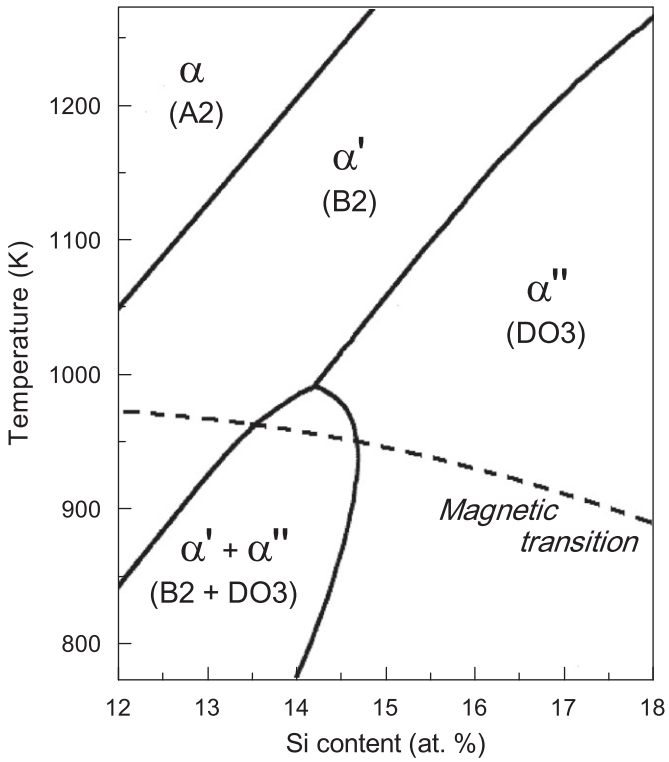

Fig. 1. Iron-rich part of the Fe–Si phase diagram [5].

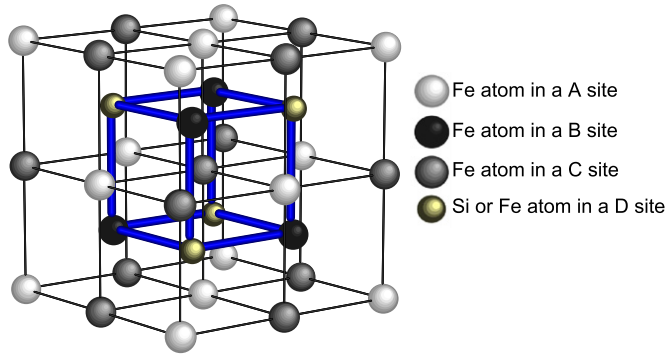

Fig. 2. Unit cell of the DO3 structure for $Fe_{1-x}Si_x$.

In $Fe_{1-x}Si_x$, Fe atoms replace some Si atoms in the D sites. Therefore, Fe [A,C] atoms have from 0 to 4 Si atoms as NN, while as next-nearest-neighbours (NNN) they have 6 Fe atoms and no Si atoms. Si [D] and Fe [D] atoms have 8 Fe atoms and no Si atoms as NN and from 0 to 6 Si atoms as NNN. Assuming that the Si atoms have an equal probability of occupying any of the D sites, the Fe atoms fraction that will occupy the different types of sites can be calculated using binomial distributions [7,8]

$$A_n = A(n,0) = \frac{0.5}{1-c}\binom{4}{n}(4c)^n(1-4c)^{4-c}; \quad n = 0,\ldots,4. \tag{1}$$

$$D_n = D(0,n) = \frac{0.5-c}{1-c}\frac{0.25}{0.5-c}\binom{6}{n}(4c)^n(1-4c)^{6-c}; \quad n = 1,\ldots,6 \tag{2}$$

$$D_0 = D(0,0) = \frac{0.5-c}{1-c}\frac{0.25-c}{0.5-c} + \frac{0.5-c}{1-c}\frac{0.25}{0.5-c}(1-4c)^6 \tag{3}$$

where c is the Si concentration, $A_n=(n, 0)$ represents a Fe [A,C] atom with n Si atoms as NN and none as NNN and $D_n=(0, n)$ represents a Fe [D] atom with no Si atoms as NN and n as NNN.

According to formulae (1)–(3), 12 different configurations exist, which have a different number of Si atoms as NN and/or NNN (i.e. A0–A4, D0–D6). These configurations can be partially resolved in the Mössbauer spectrum. If subspectra corresponding to the crystalline phase can be assigned to the various sites, then the Si concentration c in the nanocrystals can be estimated by a least squares fitting of the appropriate binomial distributions to the experimental data (the normalized percentages of Fe over the total Fe in the crystalline phase, corresponding to each type of nanocrystalline site) [8–10].

Depending on the Si content of the phase, it may be possible to separate the magnetic hyperfine fields (Bhf) corresponding to D0, D1–D6, A0, A1, A2, A3 and A4. Therefore, the fitting procedure may include as many as 7 crystalline subspectra. However, due to the complexity of the spectrum where the intensities of neighbouring subspectra are strongly overlapped, some of the subspectra are often unsolvable. Normally, a Bhf of ~32.5 T is considered for the sites with 8 Fe atoms as NNN (A0+D0) and a second Bhf of ~31 T is considered for the rest of the D sites (D1–D6). Sometimes, a third Bhf of ~30 T can be resolved for the A site with 7 Fe atoms as NN (A1). The three subspectra corresponding to A sites with 6, 5 and 4 Fe atoms as NN (A2, A3 and A4) are normally well resolved [11].

3. Magnetic moments of Fe sites in α″-$Fe_{1-x}Si_x$

Systematic behaviours of the magnetic moments of the sublattices of DO3 Fe–Si have been found when the metalloid concentration is varied: a simple rule expressed as the so-called "local-environment model" has been deduced. The model proposed by Hines et al. [12] assumes that the average moment of Fe [A,C] atoms varies linearly with Fe concentration and has particular values of +1.35 μ_B for 75.0 at% of Fe (4 Si and 4 Fe atoms as NN) and +2.20 μ_B for 100 at% of Fe (8 Fe atoms as NN), since the limit would be the BCC Fe (neglecting any variation in the lattice constant). The moment of Fe [B] and Fe [D] atoms is kept constant at +2.20 μ_B, the moment of the elemental BCC Fe, while the moment for Si [D] atoms is −0.07 μ_B. Therefore, if x is the Si fraction and $y=x\times 16$ is the number of Si atoms in the DO3 Fe–Si cell, the total moment per unit cell can be estimated as the linear combination of the moments of Fe and Si sites, as follows:

$$Fe_{1-x}Si_x = Fe[A,C]_{0.50} + Fe[B]_{0.25} + Fe[D]_{0.25-x} + Si[D]_x. \tag{4}$$

$$Fe_{(16-y)/16}Si_{y/16} = Fe[A,C]_{8/16} + Fe[B]_{4/16} + Fe[D]_{(4-y)/16} + Si[D]_{y/16} \tag{5}$$

The Fe and Si moments as well as the total moment per DO3 unit cell calculated with this local-environment model are reported in Table 1.

A similar approach was followed by Muraca et al. [13] for the system $Fe_{73.5}Si_{13.5-x}Ge_xNb_3B_9Cu_1$. However, a BCC cell was used instead of the DO3 cell and the magnetic moments of Fe [A,C] and Fe [B] atoms were taken from BCC Fe–M alloys for metalloid concentrations of less than 10 at% reported by Corb [14]; the small negative contribution of Si [D] was not considered.

So far the phenomenological model [12] has been justified by the fact that it explains trends in the observed total moments versus the composition. The *ab initio* simulation of the system $Fe_{1-x}Si_x$ was done by Kudrnovsky et al. [15] who applied the coherent-potential approximation (CPA) in combination with the tight-binding linear muffin-tin orbitals method (TB-LMTO) to the iron-rich $Fe_{1-x}Si_x$ system with fixed lattice parameter. The partial substitution of Si with Fe atoms was allowed at the D sites in the DO3 structure, (A, C) and B sites being occupied by Fe atoms

Table 1
Calculated Fe and Si moments (μ_B per atom) and the magnetization (total moment per DO3 unit cell) for $Fe_{1-x}Si_x$ ($Fe_{(16-y)/16}Si_{y/16}$) alloys taken from the literature. *Sources*: local-environment model [12], *ab initio* model [15], experimental values [16]

Source	y	Fe [A,C]	Fe [B]	Fe [D]	Si [D]	Total
Local-environment model	0	2.20	2.20	2.20	–	35.20
	1	1.99	2.20	2.20	−0.07	31.23
	2	1.78	2.20	2.20	−0.07	27.26
	3	1.56	2.20	2.20	−0.07	23.29
	4	1.35	2.20	–	−0.07	19.32
***Ab initio* model**	0	2.22	2.22	2.22	–	35.52
	1	1.85	2.27	2.23	−0.13	30.44
	2	1.67	2.35	2.27	−0.12	27.06
	3	1.38	2.43	2.29	−0.08	22.81
	4	1.10	2.52	–	−0.08	18.56
Experimental	4	1.20	2.40	–	−0.07	18.92

only. It was demonstrated that the empirical rules are consistent with a quantitative theory.

Kudrnovsky et al. have performed calculations for $Fe_{(16-y)/16}Si_{y/16}$ with $y=1$, 2, 3 and 4 (Fe_3Si). Actually, $y=1$ ($x=6.25$ at% Si) is outside the regime of the DO3 structure (α''-phase) according to the phase diagram (Fig. 1), but nevertheless they included it in the calculations in order to examine trends. The moments calculated with this *ab initio* model are also reported in Table 1. The moment of Fe [A,C] atoms varies significantly with y as described in the local-environment model. Moreover, a weak dependence on y was found for Fe [B], Fe [D] and even Si [D] atoms' moments. Note that the magnetic moment of Fe [B] atoms in the DO3 cell is actually larger than the one of Fe sites in pure α-Fe.

Experimentally, neutron-scattering data obtained at room temperature [16] yield the following sublattice moments in the ordered Fe_3Si: Fe [A,C], 1.20 ± 0.12 μ_B; Fe [B], 2.40 ± 0.06 μ_B and Si [D], -0.07 ± 0.06 μ_B. Note that even the small, negative Si moment has been found experimentally.

The *ab initio* results from [15] will be used for calculations in the present work since they not only present the linear variation of the Fe [A,C] magnetic moments with the number of Si atoms as NN, but also the negative moment of Si [D] atoms and the enhancement of the moment of Fe [B] atoms in the DO3 structure. A more adequate *ab initio* study was done by Kulikov et al. [17] who considered a variation in the lattice parameter, but it could not be applied in this work since only the magnetic moments for the ordered Fe_3Si were published.

4. Experimental

FINEMET type ribbons of compositions: (i) series I: $Fe_{73.5}Si_{13.5}B_9Nb_{3-x}Mo_xCu_1$, $x=0$, 1.5, 2, 3 (Mo0, Mo1.5, Mo2 and Mo3, respectively) and (ii) series II: $Fe_{64.8}Si_{6.2}B_{20.1}Nb_{6.7}Cu_{2.2}$ (Mo0_rem-am), $Fe_{63.4}Si_4B_{22.6}Nb_{3.7}Mo_{3.7}Cu_{2.5}$ (Mo1.5_rem-am) and $Fe_{61.8}Si_2B_{25.1}Nb_{2.8}Mo_{5.6}Cu_{2.8}$ (Mo2_rem-am) were produced by the planar flow casting technique in air. The amorphous structure on both sides and chemical compositions were checked by X-ray diffraction (XRD) and by inductively coupled plasma spectroscopy, respectively. Nanocrystallization of Fe–Si grains was induced in samples from series I by annealing in vacuum at 813 K for 1 h.

The structure of the annealed samples of series I was analysed by XRD and Mössbauer spectroscopy (MS) at room temperature. XRD was performed using a Rigaku Geiger Flex D-Max II TC diffractometer. All scans were run at 40 kV/20 mA with monochromatic radiation Cu K_α (1.5418 Å). MS was carried out in transmission geometry using a constant acceleration drive and a ^{57}Co in Rh source. The calibration was done with an α-Fe foil and isomer shifts are given relative to α-Fe.

The density of the samples was determined by the buoyancy (archimedean) method with an accuracy of $\pm 0.5\%$.

Saturation flux density magnitudes of both series I and II were measured with the conventional fluxmetric method with an accuracy of $\pm 0.5\%$.

5. Results

Mössbauer spectra were fitted under the assumption that the crystalline phase was characterized only by α''-$Fe_{1-x}Si_x$, whose presence was confirmed by XRD (Fig. 3). Okumura et al. [18] have shown that this assumption is quite plausible and it has already been used by many researchers [9,11,19–22].

Two phases were considered to fit the Mössbauer spectra: an amorphous phase represented by an asymmetric gaussian distribution of hyperfine fields and the Fe–Si crystalline phase with DO3 structure fitted with 5 subspectra corresponding to A0+D0, A1+D1 to D6, A2, A3 and A4 (Fig. 4). The relative intensities between peaks 2 and 3 (A23) were set equal for all subspectra in each sample, in order to simplify the complex fitting procedure. Parameters obtained from the Mössbauer spectra fitting are reported in Table 2.

The Si content of the crystalline phase was estimated by a least squares fitting of appropriate binomial distributions to the experimental data as described in Section 2. The comparison of the normalized percentages was made for S1+S2 (S1 and S2 could not be well resolved), S3, S4 and S5. The estimated values were 19.4, 19.8, 19.9 and 20.3 Si at% for Mo0, Mo1.5, Mo2 and Mo3, respectively. The fact that the found values were about 20 at% of Si is consistent with the assumption that the crystalline phase has a DO3 structure (Fig. 1). These values are in agreement with a decrease in the lattice parameter of Fe–Si phase observed with XRD (Table 3).

The ratio of Fe atoms in the crystalline and amorphous fractions was determined from the relative absorption areas of the Mössbauer spectra, assuming the same *f*-recoilless fractions as previously done by Borrego et al. [20–21] and Grenèche et al. [23]. From these ratios and the composition of the nanocrystals estimated by the binomial distributions fitting, the crystalline and amorphous atomic fractions were calculated (Fig. 5). As an

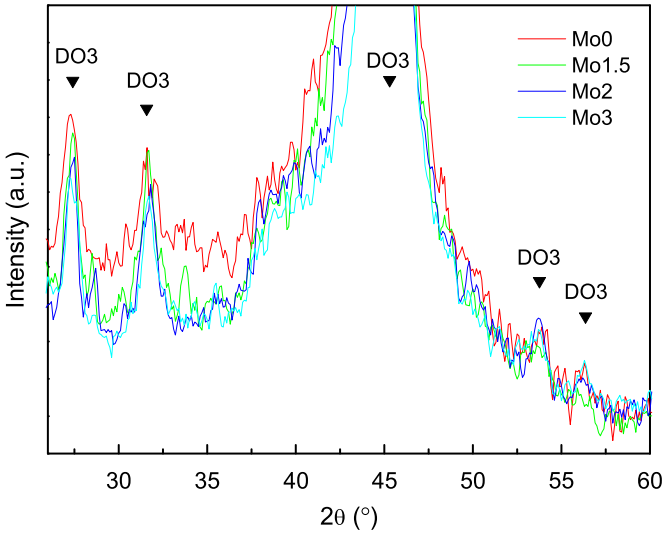

Fig. 3. X-ray diffractograms of samples annealed at 813 K for 1 h.

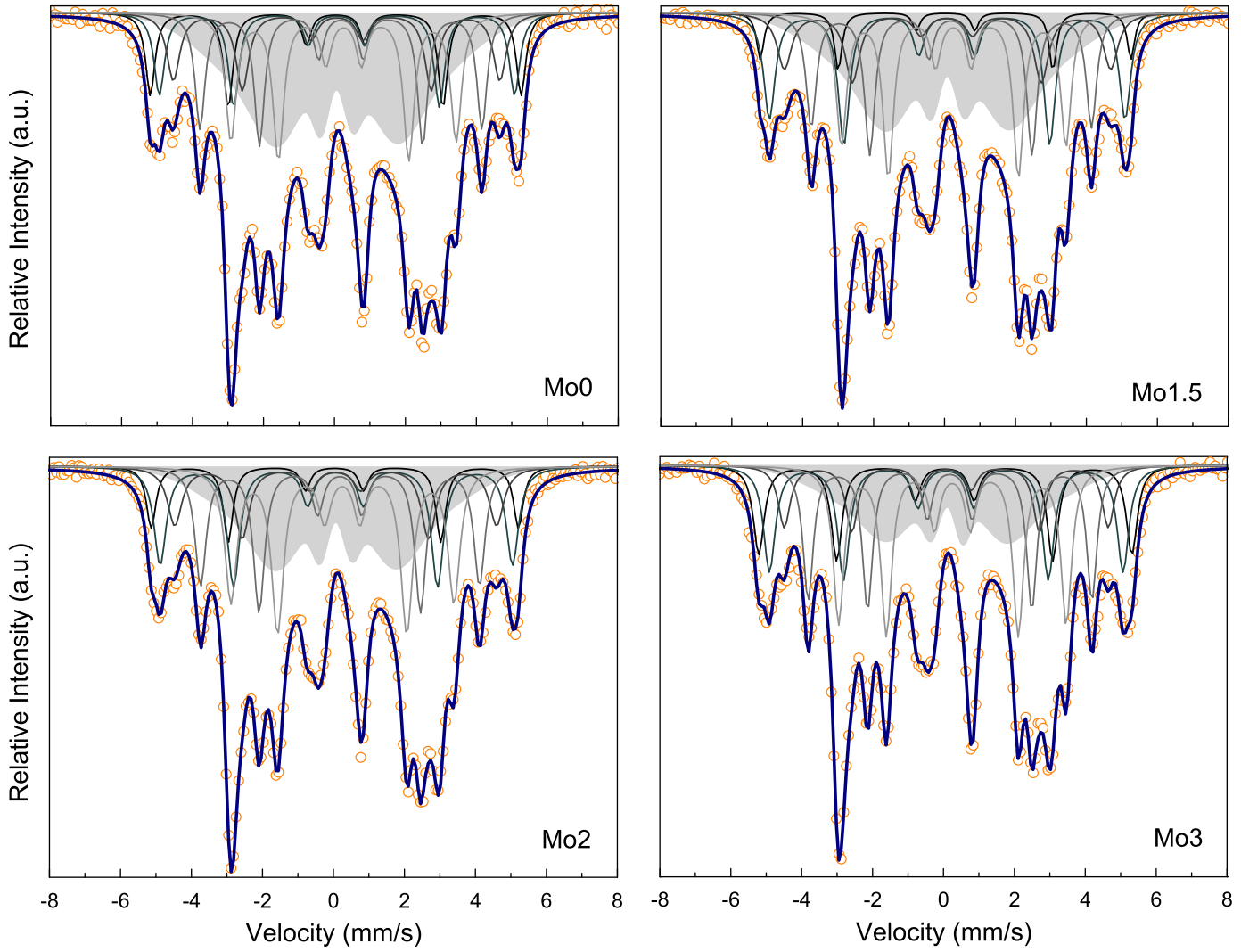

Fig. 4. Mössbauer spectra and fittings for annealed samples. Shaded subspectra represent amorphous phase, while the solid-lined spectra (S1–S5) correspond to crystalline sites.

example of the followed procedure, the calculations done for Mo0 are detailed in the appendix.

Afterwards, the chemical composition of the amorphous remaining matrix was determined. Again, some calculations performed for Mo0 are shown in the appendix as an example of the followed procedure. The chemical composition of the nanocrystalline series can be described as follows:

$$100\,Fe_{73.5}Si_{13.5}B_9Nb_3Cu_1(\text{nano}) \equiv 55.2\,Fe_{80.6}Si_{19.4}(\text{cr}) + 44.8\,Fe_{64.9}Si_{6.4}B_{19.9}Nb_{6.6}Cu_{2.2}(\text{am})$$

$$100\,Fe_{73.5}Si_{13.5}B_9Nb_{1.5}Mo_{1.5}Cu_1(\text{nano}) \equiv 60.2\,Fe_{80.2}Si_{19.8}(\text{cr}) + 39.8\,Fe_{63.3}Si_{3.8}B_{22.8}Nb_{3.8}Mo_{3.8}Cu_{2.5}(\text{am})$$

$$100\,Fe_{73.5}Si_{13.5}B_9Nb_1Mo_2Cu_1(\text{nano}) \equiv 64.1\,Fe_{80.1}Si_{19.9}(\text{cr}) + 35.9\,Fe_{61.2}Si_{1.4}B_{25.8}Nb_{2.8}Mo_{5.7}Cu_{2.8}(\text{am})$$

$$100\,Fe_{73.5}Si_{13.5}B_9Mo_3Cu_1(\text{nano}) \equiv 66.4\,Fe_{79.7}Si_{20.3}(\text{cr}) + 33.6\,Fe_{61.3}Si_0B_{26.8}Mo_{8.9}Cu_3(\text{am})$$

From a simple mass balance consideration, the atomic crystalline and amorphous fractions were converted to mass fractions, which were in turn converted to volumetric fractions with the density values. The densities of the nanocrystalline samples were measured by the buoyancy method and the densities of the crystalline grains were estimated from their chemical composition and the volume of the DO3 unit cells (calculated as the cube of the lattice parameter of the DO3 Fe–Si phase obtained from XRD). The values of these magnitudes are presented in Table 4.

Applying the *ab initio* moment's model described in Section 3 to the Fe–Si grains of known composition, we were able to calculate the magnetic moment per DO3 unit cell (μ_B/cell) and the mass magnetization contribution (emu/g) of the nanocrystals. For this purpose, a linear combination of DO3 unit cells with an integer number of Si atoms was used. For example, for Mo0 alloy, in which the chemical composition of the grains was estimated to be $Fe_{80.6}Si_{19.4}$, we used 57 out of 514 DO3 cells with 4 Si and 12 Fe atoms (type I), together with 457 out of 514 DO3 cells with 3 Si and 13 Fe atoms (type II). Type I-cells have a magnetic moment of 18.56 μ_B, whereas the moment of type II-cells is 22.81 μ_B (from *ab initio* calculations from Table 1). Therefore, the average magnetic moment of $Fe_{80.6}Si_{19.4}$ nanocrystals is $57/514 \times 18.56\ \mu_B + 457/514 \times 22.81\ \mu_B = 22.34\ \mu_B$ or 154.57 emu/g. Being 7.36 g/cm^3 the estimated density of the crystals (Table 3), the magnetic flux density B of the crystalline grains was calculated to be 1.138 T. The values of these magnitudes are reported in Table 4.

We succeeded in casting ribbons with the composition equivalent to that of the remaining amorphous matrix for the case of Mo0, Mo1.5 and Mo2 (Mo0_rem-am, Mo1.5_rem-am and Mo2_rem-am). We failed in the case of Mo3 because of the high B content; the as-quenched ribbons burnt when they came out of the melt-spinning crucible nozzle. The measured values of B of the as-quenched Mo series together with the nanocrystalline-series and the as-quenched 'remaining amorphous matrix'-series are also reported in Table 4.

The magnetic contribution of the remaining amorphous matrix (B_{sat}^{rem-am}) was estimated by solving a simple magnetic balance consideration:

$$B_{sat}^{nano} = x \times B_{sat}^{cryst} + (1-x) \times B_{sat}^{rem-am}. \quad (6)$$

where B_{sat}^{nano} is the measured value of B for the nanocrystalline sample, B_{sat}^{cryst} is the calculated B of the Fe–Si grains and x the crystalline fraction in vol%. All flux density values can be found in Table 4.

6. Discussion

A linear relation between the hyperfine field (Bhf) of the Fe [A,C] sites and the number n of Si atoms as NN was found for all the samples in agreement with already reported values [24] (Fig. 6): as the number of Si atoms as NN increases, the 3d-electron charge density at Fe-sites decreases, resulting in a decrease in the Bhf. As a first approximation, a decrease in 3.1 T per Si atom as NN was calculated. As the number of Si atoms as NN increases, the s-electron charge density at Fe-sites is reduced and hence, the isomer shift (IS) increases. Therefore, a linear correlation between IS and Bhf can be plotted (Fig. 7). Such relation is responsible for the asymmetrical shape of the spectra.

As Mo content was increased at the expense of Nb, Mössbauer fittings revealed a monotonous increase in the crystalline fraction. This behaviour was in agreement with the decrease in the thermal stability with the Nb–Mo exchange already reported in Ref. [3]. The increase in the crystalline fraction, however, did not substantially affect the present crystalline sites, i.e. all Mössbauer spectra were very similar to each other.

Regarding the chemical composition, MS showed that Si content in the nanocrystals increased when Mo in the alloy increased. It is interesting to point out that in this work, DO3 composition was modified by gradually replacing the refractory element but maintaining Fe, Si and B contents unchanged, as well as the heat treatment (813 K, 1 h). Furthermore, due to an increase in the crystalline fraction and to the Si content in the grains, a decrease in magnetostriction might be expected [25]. However, as reported in Ref. [4], such improvement was not observed in our measurements; this might have been because the variation was too small and/or because the chemical composition of the amorphous phase also changed (as will be discussed next), modifying its magnetostriction constant.

Variations in the amorphous and crystalline fractions together with modifications to the crystalline compositions, led to a change in the composition of the remaining amorphous matrix. There was a

Table 2
Hyperfine parameters obtained from the fitting: IS: isomer shift (±0.01 mm/s), Bhf: hyperfine field (±0.1 T), area: relative absorption area (±1%) and A23: alignment of the hyperfine magnetic field (±0.1). A0–A4 and D1–D6 correspond to the different Fe sites in the crystalline phase. Am corresponds to the amorphous phase.

Mo	Subspectrum	Fe site	IS (mm/s)	Bhf (T)	Area (%)	A23
0	S1	A0+D0	0.03	32.5	9	2.9
	S2	A1+D1→D6	0.06	31.1	11	
	S3	A2	0.06	28.6	10	
	S4	A3	0.19	24.7	14	
	S5	A4	0.26	19.7	16	
	S6	Am	0.07	17.6	40	
1.5	S1	A0+D0	0.03	32.5	5	3.2
	S2	A1+D1→D6	0.07	31.1	16	
	S3	A2	0.08	28.6	11	
	S4	A3	0.19	24.5	16	
	S5	A4	0.25	19.7	18	
	S6	Am	0.09	17.5	34	
2	S1	A0+D0	0.03	32.1	7	3.1
	S2	A1+D1→D6	0.07	30.8	15	
	S3	A2	0.06	28.2	11	
	S4	A3	0.18	24.4	17	
	S5	A4	0.25	19.5	21	
	S6	Am	0.07	17.0	29	
3	S1	A0+D0	0.04	32.7	12	2.7
	S2	A1+D1→D6	0.07	31.0	15	
	S3	A2	0.07	28.4	9	
	S4	A3	0.18	24.9	16	
	S5	A4	0.25	19.9	20	
	S6	Am	0.10	17.0	28	

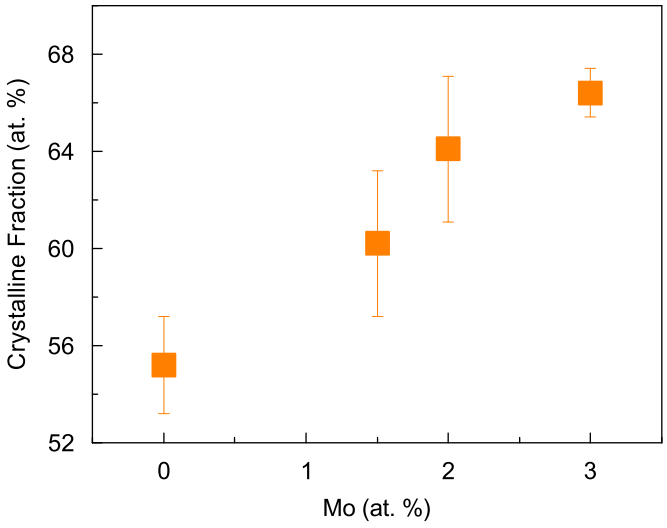

Fig. 5. Crystalline fraction (at%) of each sample.

Table 3
Estimated atomic, mass and volume crystalline and amorphous fractions.

Mo	Atomic fractions (at%)		Mass fractions (wt%)		DO3 Fe–Si Lattice parameter (Å)	Densities (g/cm^3)		Volume fractions (vol%)	
	Crystals	Amorphous matrix	Crystals	Amorphous matrix		Crystals	Nanocrystalline alloy	Crystals	Amorphous matrix
0	55.2	44.8	56.6	43.4	2.834	7.36	7.39	56.8	43.2
1.5	60.2	39.8	61.5	38.5	2.833	7.36	7.34	61.4	38.6
2	64.1	35.9	65.4	34.6	2.830	7.37	7.36	65.3	34.7
3	66.4	33.6	67.6	32.4	2.828	7.37	7.40	67.9	32.1

Note: Crystals' densities were estimated with the lattice parameters obtained from XRD. The density of the nanocrystalline alloy was measured.

Table 4
Estimated and measured magnetic values.

Mo	Crystals			Nanocrystalline alloy	Remaining amorphous matrix	Remaining amorphous matrix	As-quenched precursor
	Magnetic moment (μ_B/cell) [estimated]	Mass magnetization (emu/g) [estimated]	B (T) [estimated]	B (T) [measured]	B (T) [measured]	B (T) [estimated]	B (T) [measured]
0	22.34	154.57	1.138	1.00	0.75	0.81	1.02
1.5	22.09	153.16	1.127	1.02	0.70	0.86	1.01
2	22.00	152.65	1.126	1.04	0.67	0.87	1.01
3	21.74	151.15	1.114	1.06	–	0.96	1.03

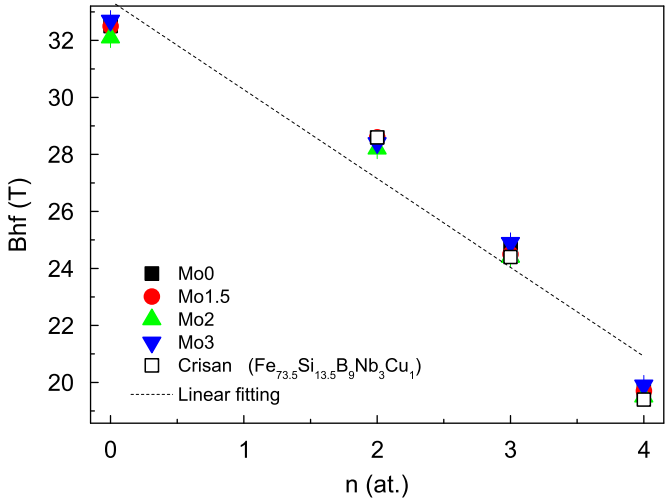

Fig. 6. Variation in the hyperfine field (Bhf) of the Fe [A,C] sites with the number of Si atoms as NN (n), together with reference data [24] and the linear fitting.

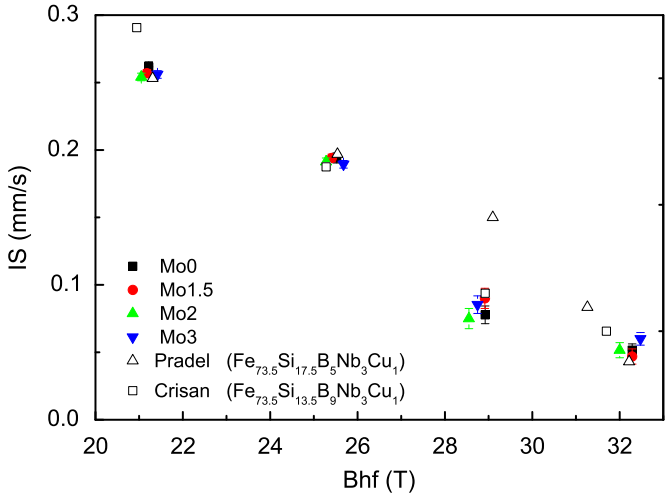

Fig. 7. Isomer shift (IS) as a function of the hyperfine field (Bhf) of the Fe [A,C] sites, together with reference data [11,24].

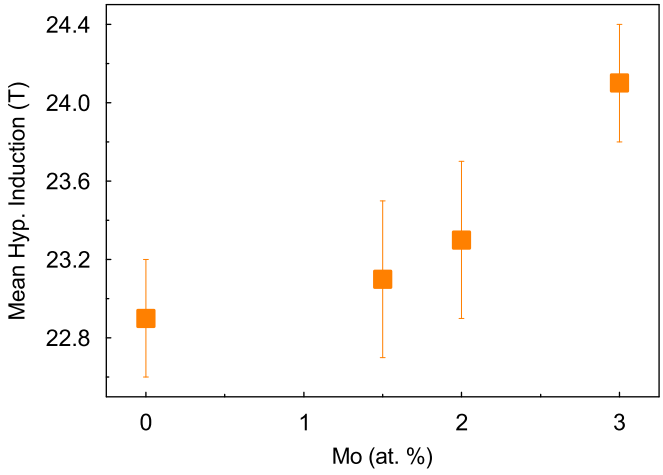

Fig. 8. Mean hyperfine induction of the samples Mo0, Mo1.5, Mo2 and Mo3.

decrease in Fe (at%) and in Si—most of which entered the nanocrystals for alloys with higher Mo contents—and an enrichment in Cu, B and the refractory elements content (Nb+Mo), since they all remained in the amorphous phase. Therefore, the properties of the remaining amorphous matrix should be different from those of the as-quenched amorphous precursor.

Although a slight increase in the magnetic induction B might be observed in alloys after the nanocrystallization, it was not as significant as to assure such variation. Due to a decrease in the Fe content in the as-quenched Mo-rem series as compared to the as-quenched Mo series, a clear decrease in B was observed (Table 4). However, an opposite behaviour was observed for the estimated B of the remaining amorphous matrices with respect to the as-quenched Mo series. This phenomenon might be an indicator of the magnetic polarization of the remaining amorphous matrix induced by the penetration of exchange fields from the crystalline grains, which compensates the expected decrease in B due to variations in chemical compositions. In fact, the difference between the estimated and the measured B was larger in alloys with more Mo content, i.e. with greater crystalline fraction, showing that the influence of the penetration fields increased as the crystalline fraction increased. Furthermore, the estimated B for the remaining amorphous matrices was higher in the alloys with more Mo content despite having less Fe content. Therefore, the use of Eq. (6) for estimating the crystalline fraction of nanocrystalline alloys as proposed by Muraca et al. [26] should be done carefully, since it does not consider the coupling between amorphous and crystalline phases. This effect was first reported by Skorvanek et al. [27], who observed that the estimated Curie temperature of the remaining amorphous matrix was higher than the measured value of a single-phase amorphous ribbon of the same chemical composition. Following the same idea, but considering the penetrating fields from the remaining amorphous matrix into the grains, a decrease in B of the crystalline phase in the nanocrystalline alloys might be expected when compared to a single-crystalline-phase α''-$Fe_{1-x}Si_x$ sample.

The mean hyperfine induction increased when the sample composition was changed from Mo0 towards Mo3 (Fig. 8). Although Mo content led to an increase in Si content in the

nanocrystals and this slightly decreased its hyperfine field, increase in the crystalline fraction counteracts the effect (the Bhf of the crystals is larger than that of the amorphous phase).

In contrast to the mentioned trends, a non-monotonous behaviour was observed for the area ratio of the second and third lines of the Mössbauer spectra, i.e. the A23 parameter: 2.92, 3.17, 3.13 and 2.71 for Mo0, Mo1.5, Mo2 and Mo3, respectively (Table 2). A23 gives information about the orientation of the magnetic moment. A value of 4, 2 or 0 indicates the in-plane, random or out-of-plane spin orientation in the sample, respectively. A preferential alignment of the local magnetic moments near the ribbon surface was found in Nb+Mo-containing alloys. It is well known that the magnetization is coupled to the stress by the magnetostriction constant. For this reason, the easy direction of a positively magnetostrictive ribbon is oriented perpendicular to the ribbon plane; however our magnetostriction measurements did not contribute to the understanding of this behaviour since no significant change was found when Nb was gradually replaced by Mo [4].

7. Conclusions

The nanocrystalline series $Fe_{73.5}Si_{13.5}Nb_{3-x}Mo_xB_9Cu_1$ was prepared, as well as a set of amorphous alloys with equivalent compositions of those of the remaining amorphous matrices. The structure and magnetic properties of the nanocrystalline system were correlated in a study that involved Mössbauer spectroscopy, X-ray diffraction, density and flux density measurements and simple balance models. There was no drastic change on the alloy structure with composition change.

The calculated phases' fractions of the nanocrystalline alloys revealed that increase in Mo content led to larger crystalline fractions, in agreement with the detriment of the thermal stability previously reported [3]. Thus, both mean hyperfine field and *B* augmented with Mo content.

The chemical compositions of both phases could be estimated and an increase in Si content in the α''-$Fe_{1-x}Si_x$ grains was observed when Nb was replaced by Mo. *Ab initio* simulations (taken from [15]) were used for the first time to calculate the magnetic contribution of FINEMETs' DO3 crystalline phase. The estimated *B* of the remaining amorphous matrices was higher than that of as-quenched amorphous samples of the same compositions. This is a further evidence of the presence of a magnetic polarization of the remaining amorphous matrix by penetrating exchange fields arising from the crystalline grains, which was larger for higher crystalline fractions. Therefore, magnetic balance considerations should be taken carefully in future works.

Finally, a preferential orientation of the net magnetization of the sample towards the surface was observed for Nb+Mo-containing samples.

Acknowledgements

We thank Beata Butvinová and Pavol Butvin for carrying out the density measurements and Juan Manuel Conde Garrido for his kind help during the preparation of this paper.

Appendix

Example of the procedure followed for calculating the crystalline and amorphous atomic fractions for Mo0:

Fe fraction in the amorphous phase ≅ relative absorption area of the subspectrum S6 = 40%

Fe fraction in the crystalline phase ≅ relative absorption area of the subspectra S1 → S5 = 60%

% Si in crystalline phase = 19.4% (from binomial distributions fitting)

% Fe in crystalline phase = 100–% Si in the crystalline phase = 100–19.4% = 80.6%

% Fe in the alloy = 73.5%

% Fe of total alloy in crystalline phase = Fe fraction in the crystalline phase × % Fe in the alloy = 60 × 73.5% = 44.1%

% Si of total alloy in the crystalline phase (directly proportional to Fe) = 44.1 × 19.4/80.6% = 10.6%

Crystalline fraction = % Fe of total alloy in the crystalline phase + % Si of total alloy in the crystalline phase = 44.1 + 10.6% = 54.7%

Amorphous fraction = 100 − 54.7% = 45.3%

Example of the procedure followed for calculating the chemical composition of the amorphous remaining matrix for Mo0:

% Fe remaining in the amorphous matrix = % Fe in the alloy − % Fe of total alloy in the crystalline phase = 73.5–44.1% = 29.4%

% Si remaining in the amorphous matrix = % Si in the alloy − % Si of total alloy in the crystalline phase = 13.5–10.6% = 2.9%

% B remaining in the amorphous matrix = % B in the alloy = 9%

% Nb remaining in the amorphous matrix = % Nb in the alloy = 3%

% Cu remaining in the amorphous matrix = % Cu in the alloy = 1%

Total at% remaining in the amorphous matrix = (29.4 + 2.9 + 9 + 3 + 1) = 45.3%

Normalized % Fe in the matrix = 29.4/45.3% = 64.9%.

An analogous procedure was followed for the other elements.

References

[1] Y. Yoshizawa, S. Oguma, K. Yamauchi, J. Appl. Phys. 64 (1988) 6044.
[2] G. Hampel, A. Pundt, J. Hesse, J. Phys.: Condens. Matter 4 (1992) 3195.
[3] J.M. Silveyra, E. Illeková, P. Svec, D. Janickovic, A. Rosales Rivera, V.J. Cremaschi, Phys. B : Condens. Matter 405 (2010) 2720.
[4] J.M. Silveyra, V.J. Cremaschi, G. Vlasák, E. Illeková, D. Janickovic, P. Svec, J. Magn. Magn. Mater. 322 (2010) 2350.
[5] S. Matsumura, Y. Tanaka, Y. Koga, K. Oki, Mater. Sci. Eng. A 312 (2001) 284.
[6] O. Ikeda, Y. Himuro, I. Ohnuma, R. Kainuma, K. Ishida, J. Alloys Compd. 268 (1998) 130.
[7] M.B. Stearns, Phys. Rev. 129 (1963) 1136.
[8] G. Rixecker, P. Schaaf, U. Gonser, Phys. Status Solidi A 139 (1993) 309.
[9] G. Rixecker, P. Schaaf, U. Gonser, J. Phys.: Condens. Matter 4 (1992) 10295.
[10] G. Rixecker, P. Schaaf, U. Gonser, Phys. Status Solidi A 151 (1995) 291.
[11] T. Pradell, J. Zhu, N. Clavaguera, M.T. Clavaguera-Mora, J. Appl. Phys. 83 (10) (1998) 5171.
[12] W.A. Hines, A.H. Menotti, J.I. Budnick, T.J. Burch, T. Litrenta, V. Niculescu, K. Raj, Phys. Rev. B 13 (1976) 4060.
[13] D. Muraca, V. Cremaschi, J. Moya, H. Sirkin, J. Magn. Magn. Mater. 320 (2008) 810.
[14] B.W. Corb, Phys. Rev. B 31 (1985) 2521.
[15] J. Kudrnovsky, N.E. Christensen, O.K. Andersen, Phys. Rev. B 43 (1991) 5924.
[16] A. Paoletti, L. Passari, Il Nuovo Cimento 32 (1964) 25.
[17] N.I. Kulikov, D. Fristot, J. Hugel, A.V. Postnikov, Phys. Rev. B 66 (2002) 014206.
[18] H. Okumura, D.E. Laughlin, M.E. McHenry, J. Magn. Magn. Mater. 267 (2003) 347.
[19] H. Aghamohammadzadeh, J.M. Williams, B.S. Parmar, H.A. Davies, M.R.J. Gibbs, Hyper Interact. C 3 (1998) 29.
[20] J.M. Borrego, A. Conde, V.A. Peña-Rodríguez, J.M. Grenèche, Hyper Interact. 131 (2000) 67.
[21] J.M. Borrego, A. Conde, I. Todd, M. Frost, H.A. Davies, M.R.J. Gibbs, J.S. Garitaonandia, J.M. Barandiarián, J.M. Grenèche, J. Non-Cryst. Solids 287 (2001) 125.
[22] D. Muraca, J. Silveyra, M. Pagnola, V. Cremaschi, J. Magn. Magn. Mater. 321 (2009) 3640.
[23] J.M. Grenèche, M. Miglierini, A. Slawska-Waniewska, Hyper Interact. 126 (2000)) 27.
[24] O. Crisan, J.M. Greneche, J.M. Le Breton, A.D. Crisan, Y. Labaye, L. Berger, G. Filoti, Eur. Phys. J. B 34 (2003) 155.
[25] G. Herzer, Handbook of Magnetic Materials, vol. 10, K.H.J. Buschow, Elsevier Science, North Holland, Amsterdam, 1997.
[26] D. Muraca, J. Moya, V.J. Cremaschi, H.R.M. Sirkin, Physica B 398 (2007) 325.
[27] I. Skorvánek, J. Kovác, J.M. Grenèche, J. Phys.: Condens. Matter 12 (2000) 9085.